JOURNAL OF COMPUTATIONAL PHYSICS 16, 240–258 (1974)

Extension of Perturbation Series by Computer: Viscous Flow between Two Infinite Rotating Disks*

GILBERT H. HOFFMAN

McDonnell Douglas Research Laboratories, McDonnell Douglas Corporation, P. O. Box 516, St. Louis, Missouri 63166

Received March 11, 1974

A digital computer is used to extend the low-Reynolds-number perturbation series for viscous, incompressible flow between two infinite, concentric, rotating disks. Ten terms are found for the case of contrarotating disks and eight for the case of one disk fixed. Convergence is found to be limited by a square root branch point at $R^2 = -1747.24$ and -215.63 for the contrarotating case and the one disk fixed case, respectively. Analytic continuation is used to extend the series for velocity profile and torque to high Reynolds numbers. Comparisons with published numerical solutions show excellent agreement. The link between the low-Reynolds-number perturbation solution and the solution at high-Reynolds-number is discussed.

I. INTRODUCTION

The problem of two rotating coaxial disks of infinite extent in a steady, viscous, incompressible fluid was first treated by Batchelor [1] who recognized that von Karman's similarity solution for a single rotating infinite disk [2] is still valid except that the Reynolds number enters as a parameter. Stewartson [3] was the first to solve the problem using a low-Reynolds-number expansion, although only the first term was published. He further presented qualitative graphs, based on the low-Reynolds-number solution, illustrating the development of boundary layers near the disks as the Reynolds number increases and gave estimates for the radii of convergence of the low-Reynolds-number series for two specific cases (contrarotating disks and one disk fixed). A clear quantitative picture of the evolution of the flow with increasing Reynolds number was given by the accurate numerical calculations of Lance and Rogers [4] and Benton [5]. A different approach was taken by Pearson [6] who calculated numerically the steady-state solution as the limit of the transient problem. For the contrarotating case he found that the solution becomes unstable as the Reynolds number increases. Mellor

* This work was performed under Air Force Office of Scientific Research Contract AF 49 (638) 1274, while the author was a graduate student at Stanford University.

et al. [7], in a very careful numerical investigation of the steady problem for the case in which one disk is fixed, discovered that the solution is not unique at infinite Reynolds number. They found that many solutions are possible corresponding to flows with an increasing number of cells. To further complicate matters, the one-cell family of solutions was found to have two branches. Tam [8], in his analytical treatment of the contrarotating case, discovered that eigensolutions exist for the high-Reynolds-number inviscid limit (core flow). The method of matched asymptotic expansions was used to construct a nonsymmetric flow similar to the one obtained numerically by Pearson at a Reynolds number of 1000.

This paper is concerned with the extension of Stewartson's low-Reynolds-number perturbation series by computer and is extracted from the thesis of Hoffman [9]. The present problem has the property that the nonlinear terms in the equations of motion are multiplied by a parameter, the Reynolds number. Thus a low-Reynolds-number perturbation solution produces an infinite sequence of linear problems each having a solution of a particularly simple form, a polynomial in the independent variable. This type of series is ideal for extension by computer. Moreover, the present series, which is expected to be limited in convergence by a nonphysical singularity, may be extended to high Reynolds number by analytic continuation. Then an answer to the question of how the low-Reynolds-number perturbation solution is linked to the solution at high Reynolds numbers can be sought.

The aims of the present work are threefold: first, to calculate enough terms of the low-Reynolds-number perturbation series by computer so that the nature and location of the nearest singularity (which limits convergence) can be determined accurately; second, to show that analytic continuation can be used effectively to extend the perturbation series to high Reynolds number; and third, to answer the question of how the low-Reynolds-number series is linked to the solution at high Reynolds number.

II. Solution by Computer

The problem considered herein is the steady flow of an incompressible viscous fluid between two parallel, infinite, coaxial, rotating disks. The configuration is shown in Fig. 1. The equations of motion are the steady Navier–Stokes equations. In nonrotating cylindrical coordinates with axial symmetry these are

$$(ru)_r + rw_z = 0, \tag{1a}$$

$$R(uu_r + wu_z - v^2/r) = -p_r + u_{rr} + (u/r)_r + u_{zz}\,, \tag{1b}$$

$$R(uv_r + wv_z + uv/r) = v_{rr} + (v/r)_r + v_{zz}\,, \tag{1c}$$

$$R(uw_r + ww_z) = -p_z + w_{rr} + w_r/r + w_{zz}\,, \tag{1d}$$

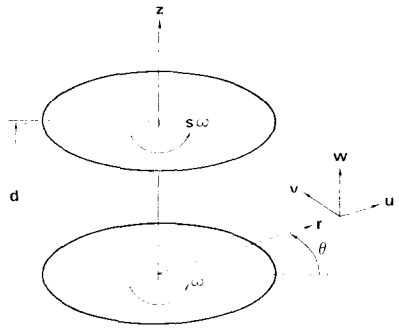

FIG. 1. Geometry for viscous flow between two rotating disks.

where (u, v, w) are velocity components in the (r, θ, z) directions, p is pressure, R is Reynolds number, and the subscripts denote partial differentiation with respect to the particular variable. Dimensionless variables are used where lengths are referred to d (the distance between disks) speeds to ωd (where ω is the rotational speed of the lower disk) and pressure to $\mu\omega$. The rotational Reynolds number, or Taylor number, R is

$$R = \rho\omega d^2/\mu, \tag{2}$$

where μ is the viscosity and ρ the density. The no-slip boundary conditions are

$$u = w = 0, \qquad v = r \quad \text{at} \quad z = 0, \tag{3a}$$

$$u = w = 0, \qquad v = sr \quad \text{at} \quad z = 1, \tag{3b}$$

where s is the ratio of disk angular velocities.

The velocity components in the self-similar form of von Karman [2] can be expressed as

$$u = -\tfrac{1}{2}Rrh'(z), \qquad v = rg(z), \qquad w = Rh(z). \tag{4}$$

These already satisfy the continuity Eq. (1a). Substitution into the momentum Eqs. (1b–d) shows that the pressure has the form (cf. [10, p. 157])

$$p = R(\tfrac{1}{2}\lambda r^2 + h' - \tfrac{1}{2}R^2h^2) + \text{const}, \tag{5}$$

where $\lambda = \lambda(R)$. After elimination of λ by differentiation, the functions g and h satisfy

$$g'' = R^2(hg' - h'g), \tag{6a}$$

$$h'''' = 4gg' + R^2hh''', \tag{6b}$$

with boundary conditions

$$g(0) = 1, \qquad h(0) = h'(0) = 0, \tag{7a}$$

$$g(1) = s, \qquad h(1) = h'(1) = 0. \tag{7b}$$

The normalization was chosen so that the problem is in a form appropriate for a small-Reynolds-number perturbation solution. The appearance of R^2 in Eq. (6) suggests that the perturbation series for g and h progress in powers of R^2 as follows:

$$g(z; R) = \sum_{n=0}^{\infty} R^{2n} g_{n+1}(z), \tag{8a}$$

$$h(z; R) = \sum_{n=0}^{\infty} R^{2n} h_{n+1}(z). \tag{8b}$$

The sequence of equations for g_i and h_i are obtained by substituting the above series into Eqs. (6a) and (6b), then equating coefficients of like powers of R^2:

$$g_1'' = 0, \tag{9a}$$

$$g_{n+1}'' = \sum_{k=1}^{n} (h_k g'_{n+1-k} - h_k' g_{n+1-k}), \qquad n = 1, 2,..., \tag{9b}$$

and

$$h'''' = 4 g_1 g_1', \tag{9c}$$

$$h''''_{n+1} = 4 \sum_{k=1}^{n+1} g_k g'_{n+2-k} + \sum_{k=1}^{n} h_k h''''_{n+1-k}, \qquad n = 1, 2,.... \tag{9d}$$

Similarly, the boundary conditions become

$$\begin{aligned} &g_1(0) = 1, \quad g_n(0) = 0, \quad n = 2, 3,..., \\ &h_n(0) = h_n'(0) = 0, \quad n = 1, 2, 3,..., \end{aligned} \tag{10a}$$

and

$$\begin{aligned} &g_1(1) = s, \quad g_n(1) = 0, \quad n = 2, 3,..., \\ &h_n(1) = h_n'(1) = 0, \quad n = 1, 2, 3,... . \end{aligned} \tag{10b}$$

The solution for the leading terms in Eq. (8) was first given by Stewartson [3]

who showed that h_1 and g_1 are polynomials in z with coefficients that are polynomials in s, viz,

$$g_1 = 1 + (s - 1)\, z, \tag{11a}$$

$$h_1 = (s - 1)\{[(1/6) + (1/15)(s - 1)]\, z^2 - [(1/3) + (1/10)(s - 1)]\, z^3 + (1/6)\, z^4 + (1/30)(s - 1)\, z^5\}. \tag{11b}$$

In fact, all succeeding g_i and h_i are polynomials in z with coefficients that are polynomials in s. Thus the inhomogeneous terms in Eqs. (9b) and (9d) are found by inspection to be of the form

$$\left.\begin{aligned} g''_{n+1} &= \sum_{k=1}^{P_n} X_k^{(n)} z^k, \qquad (12a)\\ h''''_{n+1} &= \sum_{k=1}^{Q_n} Y_k^{(n)} z^{k-1}, \qquad (12b) \end{aligned}\right\} \quad n = 1, 2,\ldots,$$

where P_n and Q_n are integers depending on n, to be determined. Integration of these equations plus satisfaction of the no-slip boundary conditions gives the solution as

$$g_{n+1}(z) = A_1^{(n+1)} z + \sum_{k=1}^{P_n} A_{k+1}^{(n+1)} z^{k+2}, \tag{13a}$$

$$h_{n+1}(z) = B_1^{(n+1)} z^2 + B_2^{(n+1)} z^3 + \sum_{k=1}^{Q_n} B_{k+2}^{(n+1)} z^{k+3}, \tag{13b}$$

where

$$A_1^{(n+1)} = -\sum_{k=1}^{P_n} \frac{X_k^{(n)}}{(k+1)(k+2)},$$

$$A_k^{(n+1)} = \frac{X_k^{(n)}}{(k+1)(k+2)}, \qquad k = 2, 3,\ldots, P_n,$$

and

$$B_1^{(n+1)} = \sum_{k=1}^{Q_n} \frac{Y_k^{(n)}}{(k+1)(k+2)(k+3)},$$

$$B_2^{(n+1)} = -\sum_{k=1}^{Q_n} \frac{Y_k^{(n)}}{k(k+2)(k+3)},$$

$$B_{k+2}^{(n+1)} = \frac{Y_k^{(n)}}{k(k+1)(k+2)(k+3)}, \qquad k = 1, 2,\ldots, Q_n.$$

The task for the computer is to perform the tedious algebra required for the determination of the coefficients $X_k^{(n)}$ and $Y_k^{(n)}$ as well as to determine the integers P_n and Q_n. In the present case, recursion relations for the coefficients $A_k^{(n+1)}$ and $B_k^{(n+1)}$ can be determined by hand without too much difficulty. These recursion relations must be evaluated by computer because of their complexity. Compared to the present method, this latter procedure naturally takes much less computer time to determine a given number of terms of the expansion.

Note that the A_k and B_k in the present treatment depend implicitly on the parameter s. This has been done to simplify bookkeeping and to reduce computer storage requirements.

In the determination of the coefficients $X_k^{(n)}$ and $Y_k^{(n)}$, the computer performs the differentiation and algebra indicated in Eqs. (9b) and (9d) and then compares the result with the polynomial forms given by Eqs. (12a) and (12b) to determine $X_k^{(n)}$ and $Y_k^{(n)}$. The details of this procedure are given in Hoffman [9].

An adaptation of the algorithm for polynomial algebra described in Hoffman [9] is used. This involves reducing the number of variables from two to one; otherwise the manipulative technique is the same. In the present problem, an efficient algorithm could be developed by taking advantage of the simple and ordered form of the polynomial involved. Double precision arithmetic is used in the coefficient calculations.

III. Results and Discussion

Solutions for $s = -1$ (contrarotating disks) and $s = 0$ (one disk fixed) have been obtained. These cases were chosen for two reasons. First, they have an extensive literature which includes solutions obtained by numerical methods, and second, the character of the flow in the two cases is sufficiently different to provide a good test of the range of applicability of the perturbation solution.

Ten terms in the series for $s = -1$ were computed, while only eight were computed for $s = 0$, for reasons to be given later. Computation time on an IBM 360/67 was 18 min for ten terms and 4.5 min for eight terms.

Estimates for the radius of convergence and the type of singularity of the series for g and h can be obtained from knowledge of a limited number of terms by the graphical method of Domb and Sykes [11]. They appear to have been the first to use this graphical technique in connection with their work on ferromagnetic susceptibility. In this method the ratio of coefficients in a series, a_n/a_{n-1}, is plotted versus $1/n$. This is suggested by the power series expansion,

$$f(x) = \sum_{n=0}^{\infty} a_n x^n = \begin{cases} C(x_0 \pm x)^\alpha, & \alpha \neq 0, 1, \ldots, \\ C(x_0 \pm x)^\alpha \ln(x_0 \pm x), & \alpha = 0, 1, \ldots, \end{cases} \tag{14a}$$

where

$$a_n/a_{n-1} = \mp[1 - (1 + \alpha)(1/n)](1/x_0). \tag{14b}$$

The intercept gives the reciprocal of the radius of convergence, while the slope at the intercept is related to the type of singularity that limits convergence.

The series for g and h presumably are uniformly convergent since the flowfield is well behaved everywhere at low Reynolds numbers. Hence the radius of convergence should be independent of location in the interval $0 \leqslant z \leqslant 1$. Results obtained independently by Van Dyke, to be described shortly, confirm that this is the case. In the present work, the radii of convergence for the g and h series

TABLE I

Coefficients Used in Domb–Sykes Plot, $s = -1$

n	$A_1^{(n)}$	$B_3^{(n)}$	a_n/a_{n-1}
2	-0.95238×10^{-3}	-0.15873×10^{-3}	
3	0.22799×10^{-6}	0.37998×10^{-7}	-2.394×10^{-4}
4	-0.75516×10^{-10}	-0.12586×10^{-10}	-3.312×10^{-4}
5	0.28689×10^{-13}	0.47815×10^{-14}	-3.799×10^{-4}
6	-0.11811×10^{-16}	-0.19684×10^{-17}	-4.116×10^{-4}
7	0.51298×10^{-20}	0.85497×10^{-21}	-4.343×10^{-4}
8	-0.23155×10^{-23}	-0.38592×10^{-24}	-4.514×10^{-4}
9	0.11685×10^{-26}	0.19474×10^{-27}	-5.046×10^{-4}
10	-0.22115×10^{-29}	-0.36858×10^{-30}	-1.893×10^{-3}

TABLE II

Coefficients Used in Domb–Sykes Plot, $s = 0$

n	$A_1^{(n)}$	$B_3^{(n)}$	a_n/a_{n-1}
2	-0.42857×10^{-2}	-0.71429×10^{-3}	
3	0.81791×10^{-5}	0.13632×10^{-5}	-1.908×10^{-3}
4	-0.22036×10^{-7}	-0.36727×10^{-8}	-2.694×10^{-3}
5	0.68471×10^{-10}	0.11412×10^{-10}	-3.107×10^{-3}
6	-0.23085×10^{-12}	-0.38475×10^{-13}	-3.371×10^{-3}
7	0.82121×10^{-15}	0.13687×10^{-15}	-3.557×10^{-3}
8	-0.30350×10^{-17}	-0.50583×10^{-18}	-3.696×10^{-3}

were determined at $z = 0$ using the coefficients $A_1^{(n)}$ and $B_3^{(n)}$. The coefficient $A_1^{(n)}$ is $g_n'(0)$ which is related to the torque series on the lower disk, whereas the coefficient $B_3^{(n)}$ is $h_n'''(0)/4!$. These coefficients are tabulated in Table I for $s = -1$ and Table II for $s = 0$ beginning with $n = 2$ where the sign pattern of the series is established. Only one column, a_n/a_{n-1}, is shown for the ratio of coefficients since both series give the same value, to the number of decimals shown, for a given n. This implies that their radii of convergence are identical for a given s.

Domb–Sykes plots for the ratio a_n/a_{n-1} are presented in Figs. 2 and 3 for $s = -1$ and $s = 0$, respectively. A regular pattern of alternating signs in these coefficients was established in both cases after $n = 2$, indicating that the singularity was on the negative axis of R^2. This singularity, therefore, is nonphysical and may be removed by a Euler transformation or other suitable means.

For $n = 9$ and 10 in Fig. 2, the points depart abruptly from the established pattern with the ninth term being about 6% high and the tenth term completely off the plot, $a_{10}/a_9 = -1.893 \times 10^{-3}$. This behavior is attributed to round-off error which was verified by repeating the calculations using single precision arithmetic. These results begin to deviate from the double precision values by $n = 4$ as shown in Fig. 2. Thus, based on experience gained with the $s = -1$ case, only eight terms were computed for $s = 0$.

The radii of convergence, in terms of Reynolds number, are 41.8 and 14.7 for $s = -1$ and 0, respectively. These values were calculated from the intercepts

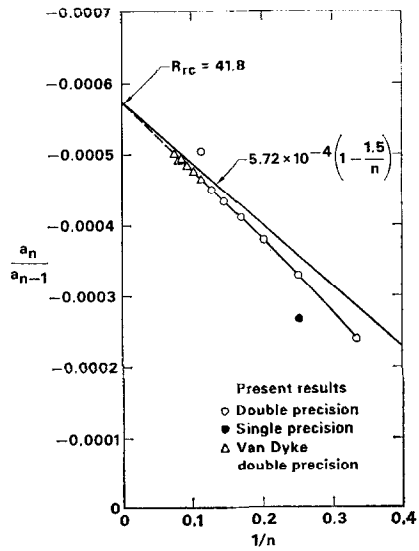

FIG. 2. Domb–Sykes Plot of $g'(0)$ or $h'''(0)$ coefficients, $s = -1$.

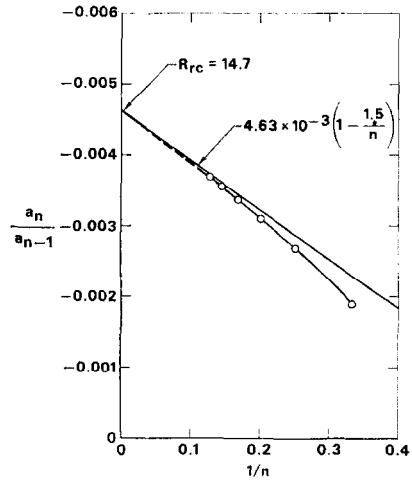

FIG. 3. Domb–Sykes Plot of $g'(0)$ or $h''''(0)$ coefficients, $s = 0$.

of the Domb–Sykes plots in Figs. 2 and 3, which in turn were determined by fitting the points $n = 3$–8 with a Lagrange polynomial with its slope constrained at the intercept. The present values for the radii of convergence are close to those given by Stewartson [3] who estimated the series to be convergent for R less than about 40 and 10 for $s = -1$ and 0, respectively.

As mentioned earlier, the limiting slope of the Domb–Sykes plot indicates the nature of the nearest singularity. This is $-(1 + \alpha)$ in Eq. (14b) where α is the exponent of the singularity. In both Figs. 2 and 3, α appears to be approaching 1/2. This value was used as the constraint in the Lagrange polynomial curve fit mentioned above. The asymptotic behavior of $g'(0)$ and $h''''(0)$, as indicated by the Domb–Sykes plot, for both $s = -1$ and $s = 0$, is therefore,

$$g'(0) \quad \text{or} \quad h''''(0) \sim \text{const}(R_{rc}^2 + R^2)^{1/2}. \tag{15}$$

For the present problem, as mentioned in Section 2, recursion relations can be derived for the coefficients in the perturbation series Eq. (8). Subsequent to the present work, Van Dyke [12] has done this for the case $s = -1$ and made his unpublished results available to the author. These recursion relations were evaluated on an IBM 360/67 computer using double precision arithmetic. Twenty terms were calculated in 2.5 min. Oscillations appeared in the lead coefficient of the g_n polynomials beginning at the 15th term, indicating that round-off error was beginning to have an effect. The h_n polynomials were not investigated.

Van Dyke's origin of coordinates was taken at the point of antisymmetry, $z = 1/2$ in present notation. Therefore, the determination of g_n' on the lower

disk requires polynomial summation at that point, a procedure which introduces additional round-off error. These values for $g_n'(0)$ through $n = 15$ are shown in Fig. 2 and coincide with present results through $n = 8$. A noticeable oscillation appears at $n = 13$. A Domb–Sykes plot of his first 15 lead coefficients for g, corresponding to $g'(1/2)$, gives the radius of convergence as 42.14. This differs from the present value of 41.7, obtained with eight terms, by 0.8 %.

Velocity Profiles

Several accurate numerical solutions of the present problem have been published in recent years ([4–6]). For comparison with present results, the most appropriate are those of Lance and Rogers [4] who present detailed numerical calculations for a fairly wide range of Reynolds numbers and for several values of s (including $s = 0$ and -1).

Before a comparison can be made, however, the velocity components appropriate to high Reynolds number (for which a limit exists as $R \to \infty$) must be expressed in terms of those at low Reynolds number. Then this result, expressed in terms of the appropriate perturbation series, is recast by appropriate means to increase its radius of convergence. The effect of two methods of analytic continuation, the Euler transformation and the use of rational fractions, will be illustrated in terms of the "reduced" azimuthal velocity component v/r, denoted by $\bar{v}$.

The perturbation series for $\bar{v}$ written in terms of a normalized expansion parameter ϵ is

$$\bar{v}(z; R) = g(z; R) = \sum_{n=1}^{\infty} \bar{g}_n(z)\, \epsilon^{n-1}, \tag{16}$$

where

$$\bar{g}_n(z) = R_{rc}^{2(n-1)} g_n(z),$$

$$\epsilon = (R/R_{rc})^2.$$

Note that $\bar{v}$ is appropriate to both high and low Reynolds numbers without modification. Also, the coefficients $\bar{g}_n$ are now $O(1)$.

The Euler transformation is defined by

$$\delta = \epsilon/(1 + \epsilon). \tag{17}$$

Equation (16) is recast in terms of the new parameter δ which removes the original singularity to $R = \infty$. If other singularities are present they will be mapped closer to the origin. This does not happen here, however.

Reduced azimuthal velocity profiles were computed for several Reynolds numbers for $s = -1$ and 0. The first eight partial sums for $\bar{v}$ were calculate from both unrecast series, Eq. (16), and recast series. As long as $R < R_{rc}$, these results

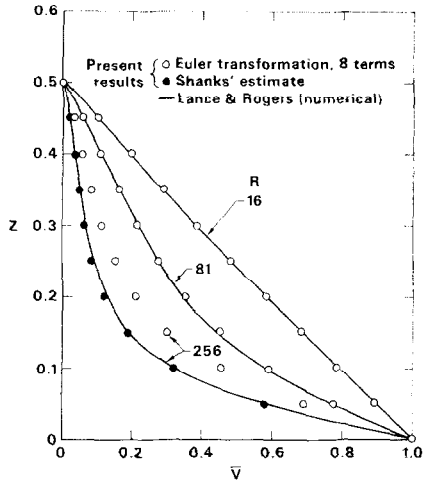

FIG. 4. Comparison of azimuthal velocity profiles at various Reynolds numbers from present theory with numerical solutions of Lance and Rogers, $s = -1$.

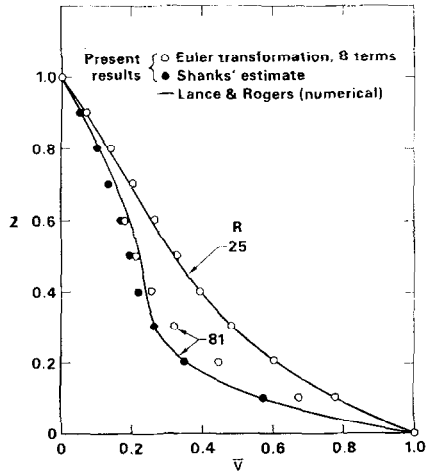

FIG. 5. Comparison of azimuthal velocity profiles at various Reynolds numbers from present theory with numerical solutions of Lance and Rogers, $s = 0$.

differ little. For $R > R_{rc}$, the unrecast results are meaningless, as would be expected, while the recast partial sums converge smoothly. A comparison between eight terms of the Euler transformed perturbation solution for $\bar{v}$ and the numerical results of Lance and Rogers [4] is shown in Fig. 4 for $s = -1$ and in Fig. 5 for $s = 0$. Profiles at several Reynolds numbers appear on each plot. Since the case

$s = -1$ is antisymmetric, only half of the profile is shown. For $s = -1$ at $R = 16$ and 81, and for $s = 0$ at $R = 25$, the agreement is excellent. Reynolds numbers of 256 for $s = -1$ and 81 for $s = 0$ are well beyond the radii of convergence of the original series. At the highest Reynolds numbers in Figs. 4 and 5, eight terms of the recast series are not enough to produce a result close to convergence. Therefore, to obtain an estimate of the converged profile the first eight partial sums at these Reynolds numbers were subjected to the nonlinear transformation of Shanks [13]. This estimate is shown by filled circles in Figs. 4 and 5. The values obtained from Shanks' transformation for both $s = -1$ and 0 agree well with the result of Lance and Rogers, although for $s = 0$ the perturbation solution tends to overshoot the development of the constant-velocity core.

The second method used to improve the convergence of the perturbation series for $\bar{v}$ is rational fractions (Padé approximants). The procedure is first to remove the square root branch point that limits convergence, and then recast the remainder in a rational fraction. The virtue of rational fractions as a means of analytic continuation is that a good estimate for the sum of a series can be obtained from only a few terms. The mathematical theory can be found in Baker [14].

The (N, M) Padé approximant of the power series for $f(x)$ is

$$\frac{A_1 + A_2x + A_3x^2 + \cdots + A_Mx^M}{1 + B_1x + B_2x^2 + \cdots + B_Nx^N}. \tag{18}$$

The expansion of this rational fraction in a power series must match the original power series term-by-term up through x^{M+N}. For present purposes, x corresponds to the expansion parameter ϵ, and $f(x)$ has a finite limit as $\epsilon \to \infty$. For a finite limit, the condition $N = M$ must be imposed on the Padé approximant.

The reduced azimuthal velocity $\bar{v}$, with square root branch point removed, is given by

$$\bar{v}/(1 + \epsilon)^{1/2} = g(z; \epsilon)/(1 + \epsilon)^{1/2} = G(z; \epsilon). \tag{19}$$

The series for G was determined from the present eight terms for g. Best results in recasting G were obtained from a rational fraction with numerator and denominator of the same degree, three. To recover $\bar{v}$, the rational fraction for G is multiplied by $(1 + \epsilon)^{1/2}$.

Figures 6 and 7 compare the results of analytic continuation by Euler transformation and rational fractions for $s = -1$ and 0, respectively, at the same Reynolds numbers shown in Figs. 4 and 5. For the highest Reynolds numbers considered ($R = 256$ for $s = -1$ and $R = 81$ for $s = 0$) rational fractions are slightly superior to the Euler transformation away from $z = 0$. For the lower Reynolds numbers in Figs. 6 and 7 the two methods give practically the same results.

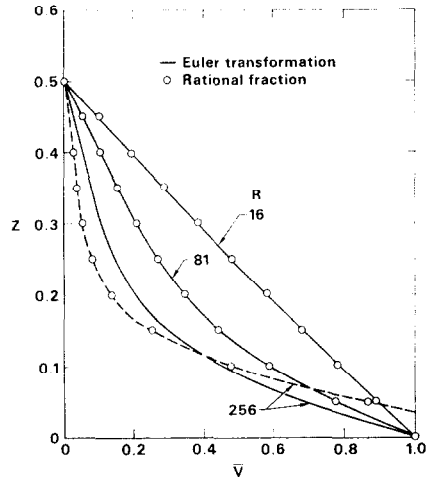

FIG. 6. Comparison of rational fractions with Euler transformation on eight terms of azimuthal velocity profile series at various Reynolds numbers, $s = -1$.

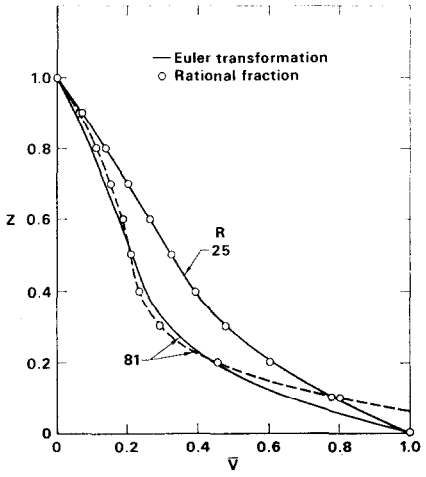

FIG. 7. Comparison of rational fractions with Euler transformation on eight terms of azimuthal velocity profile series at various Reynolds numbers, $s = 0$.

For the highest values of Reynolds number shown in Figs. 6 and 7, the rational fractions (dotted line) fail severely near $z = 0$. An overshoot, $\bar{v} > 1$, is predicted in this region. The no-slip condition is satisfied at $z = 0$, however. The reason for this behavior is not known.

Torque on Lower Disk

The nondimensional torque on the lower disk in the form given by Lance and Rogers [4] approaches a constant value as Reynolds number becomes large. This feature is very useful as a test of the power of analytic continuation of the low-Reynolds-number perturbation series. Since the disk is infinite, so is the total torque developed on it. A finite torque, however, may be defined by considering an arbitrary finite radius r_0^*. In the notation of Lance and Rogers this is

$$T^* = \mu^* \int_0^{r_0^*} v_z^* \,|_{z^*=0}\, 2\pi r^{*2}\, dr^* = -\left(\frac{\pi}{2}\,\omega^{3/2}\rho^{*1/2}\mu^{*1/2}r_0^{*4}\right) T, \tag{20}$$

where an asterisk denotes a dimensional quantity. The quantity T is a nondimensional torque and corresponds to $2^4 b$ plotted in Lance and Rogers' Fig. 2. In present notation, T is given by

$$T = -g'(0)/R^{1/2}. \tag{21}$$

In evaluating Eq. (21) using the low-Reynolds-number perturbation series, an Euler transformation will be applied to extend the radius of convergence. This transformation must be applied to the denominator $R^{1/2}$ as well. The recast series for T has the following form:

$$T = -(R_{rc}^2\delta)^{-1/4} \sum_{n=1}^{\infty} T^{(n)}\delta^{n-1}. \tag{22}$$

TABLE III

Torque Coefficients in Euler-Transformed Series

	$T^{(n)}$	
n	$s = -1$	$s = 0$
1	2.00000	1.00000
2	1.21429	0.67414
3	0.35952	0.21905
4	0.16333	0.10718
5	0.088548	0.062776
6	0.053236	0.040825
7	0.034273	0.028443
8	0.023180	0.020805

The first eight $T^{(n)}$ coefficients have been computed for $s = -1$ and 0 and are given in Table III. The values used for R_{rc}^2 in Eq. (22) are 1800.00 and 215.63 for $s = -1$ and 0, respectively. The first value, 1800, has been rounded off from $(14.7)^2$ and seems to make little difference in the convergence of the recast result.

The first eight partial sums for T have been computed for $s = -1$ and $s = 0$. These are plotted versus $R^{1/2}$ in Fig. 8 for $s = -1$ and Fig. 9 for $s = 0$. Shown for comparison are the numerical results of Lance and Rogers. In both cases the recast partial sums for T converge smoothly throughout the Reynolds number range considered ($R \leqslant 625$) and approach a constant asymptote. For $s = -1$

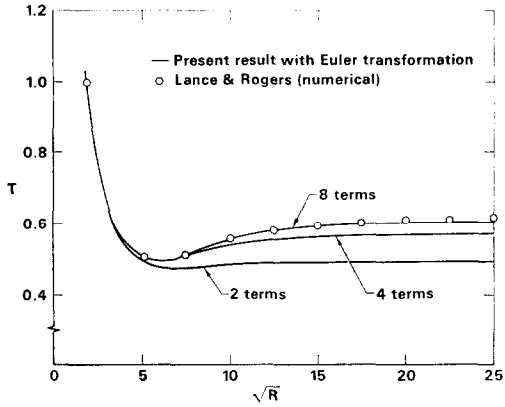

FIG. 8. Comparison of torque on lower disk vs Reynolds number from present theory with numerical solution of Lance and Rogers, $s = -1$.

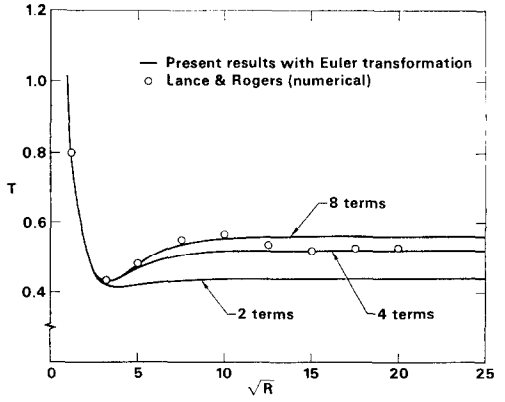

FIG. 9. Comparison of torque on lower disk vs Reynolds number from present theory with numerical solution of Lance and Rogers, $s = 0$.

the eighth partial sum agrees extremely well with Lance and Rogers' calculations over the entire range of Reynolds number shown. For $s = 0$, however, the eighth partial sum approaches a higher asymptote than Lance and Rogers' result and does not show their dip at higher Reynolds number. Apparently eight terms are not enough to reproduce accurately the value of T at the higher Reynolds numbers. This is not surprising since examination of the velocity profiles calculated by Lance and Rogers [4] and Benton [5] confirms that the $s = 0$ case has a complicated irregular behavior as R grows larger, while the $s = -1$ case remains well behaved.

IV. Perturbation Solution in Perspective

The behavior of the flow at high Reynolds number must be understood first in order to answer the question posed in the introduction, "How is the low-Reynolds-number perturbation solution linked to the high-Reynolds-number solution?" This can be accomplished by a thorough examination of the considerable literature on the subject. Then the perturbation solution can be put in perspective, at least for the two cases considered here.

The theme of all that followed concerning this problem was set by Batchelor [1]. By setting up the equations of motion and through physical reasoning, he arrived at a qualitative description of the flow fields encountered, including the two cases considered here. These were illustrated by sketches of the streamline patterns. Partly because of the unusual nature of some of Batchelor's conclusions concerning the flow behavior at high Reynolds number, other investigators were led to examine the problem both theoretically and experimentally. Since the two cases ($s = 0$ and -1) are different in flow-field character, as well as to extent covered in the literature, they can best be examined separately.

One Disk Fixed ($s = 0$)

Batchelor's view of this case at high Reynolds number was that viscous effects are confined to thin boundary layers near the disks, while the flow outside these layers is essentially inviscid and rotates with nearly constant angular speed in the same direction as the rotating disk. The rotational speed of the core is that value, lower than the rotational speed of the rotating disk, which provides a matching of the axial velocity of the inflow to the boundary layer on the rotating disk with that of the outflow from the boundary layer on the fixed disk. The boundary layer on the rotating disk corresponds to the one-disk solution of von Karman [2] generalized for a uniformly rotating flow at infinity, while the boundary layer on the fixed disk corresponds to the solution found by Bödewadt [15]. The inviscid core then rotates uniformly having streamlines which spiral from

the fixed to the rotating disk. Stewartson [3] offered an alternate view of the behavior at high Reynolds number which he based on the behavior of the perturbation solution at low-Reynolds-number and numerical investigations. His idea was that the nearly inviscid core is not rotating, and only a boundary layer on the rotating disk exists which corresponds to von Karman's original similarity solution of 1921. The subsequent investigations of Lance and Rogers [4] and of Benton [5], which were numerical integrations of Batchelor's similarity solution, clearly showed that as the Reynolds number becomes larger (of the order of 1000), the solution obtained corresponds to Batchelor's idea. Pearson [6] treated the unsteady analog of Batchelor's similarity solution and obtained the steady-state case as the limit for large time. His steady-state limit for $R = 1000$ again confirmed Batchelor's idea. The two views of Batchelor and Stewartson were brought into proper focus by Mellor *et al.* [7] who made a careful numerical investigation of Batchelor's similarity solution for the case at hand only. They found that a high Reynolds number a great number of solutions are possible, a fact not known before. These correspond to an increasing multiple of cells in the flow. For the one-cell branch they verified that Batchelor's original idea for the behavior at high Reynolds number is the actual limit reached by starting at zero Reynolds number. They also identified a second subbranch of the one-cell flows which begins at infinite Reynolds number, decreases to a minimum, and increases to infinite Reynolds number again. The first limit at infinite Reynolds number is similar to Batchelor's idea except that the inviscid core is rotating uniformly in a direction opposite to the rotating disk. The second limit at infinite Reynolds number is that conceived by Stewartson [3], namely, a nonrotating inviscid core with the solution of von Karman at the rotating disk. Mellor *et al.* also carried out a careful experimental investigation using a hot wire anemometer and found that only the first one-cell branch of solutions (Batchelor's limit) is obtained.

The place of the low-Reynolds-number perturbation solution for $s = 0$ in the Reynolds number spectrum is now clear. The agreement obtained in the comparisons of the present solution with the numerical solutions of Lance and Rogers [4] shows clearly in the context of the previous discussion that the analytic continuation of the low-Reynolds-number perturbation solution has as its high-Reynolds-number limit the flow envisioned by Batchelor. This is the first subbranch of the one-cell solutions discussed by Mellor *et al.* In addition, this is the situation realized experimentally. Although the limit as $R \to \infty$ described by Stewartson is now known to exist mathematically, it does not lie on a continuation of the low-Reynolds-number solution as Stewartson originally thought.

Contrarotating Disks ($s = -1$)

For this case Batchelor's conclusion about the limit at high Reynolds number was startling. He predicted that, as in the previous case, the viscous effects would

be confined to thin boundary layers near each disk. Outside these boundary layers, the flow would be nearly inviscid and rotating uniformly. There would be, however, two distinct inviscid cores, one associated with each disk and rotating in the same direction as that disk. In the region of the midplane, where the flow divides, viscous effects would again be important. This is necessary to account for the adjustment of the flow between two contrarotating cores. Batchelor mentioned that this solution might not be realized experimentally. The qualitative experiment of Stewartson [3] lent support to Batchelor's doubts. Stewartson used a simple apparatus which consisted of two smooth cardboard disks, 6 in. in diameter, mounted in lathe chucks. The motion of the fluid between the disks was indicated by a "light smooth propellor and a piece of cotton wool attached to a thread." The disks were rotated rapidly in the same direction until solid body rotation in the core was achieved. Then one of the disks was suddenly reversed in direction and given the same speed as before. According to Batchelor's prediction a contrarotating core would be set up; instead, the core was found to come to rest almost immediately. Further, Stewartson was able to show theoretically that an inviscid core without rotation, but with a uniform radial inflow, is possible which matches by continuity the outflow in the disk boundary layers.

The work of Lance and Rogers [4] gave additional support to Stewartson's view of the limit at high Reynolds number. Their solutions, as mentioned for $s = 0$, were numerical integrations of Batchelor's similarity solution. The highest Reynolds number at which they carried out a solution in the contrarotating case was 1023. At this value their solution shows the core region to be approaching a uniform nonrotating state with a uniform radial inflow as predicted by Stewartson.

Pearson [6] also investigated this case in the manner described previously. For $R = 100$ his steady-state solution is definitely tending toward Stewartson's limit; however, at $R = 1000$ he found that no stable symmetric solution exists (at least to one-dimensional disturbances). Instead, he found an unsymmetrical flow in which the main body of fluid is rotating in the same sense as one of the disks but at a higher angular speed. This flow can be reversed depending upon which disk is started first.

Tam [8], who investigated the asymptotic behavior of the contrarotating case, has shown the existence of eigensolutions to the equations governing the inviscid limit for large Reynolds number (flow in the core). By combining the Stewartson-type solution with one of these eigensolutions, plus using the method of matched asymptotic expansions, Tam obtained an unsymmetric solution with the same features as Pearson's steady-state limit at $R = 1000$. Tam also states that many other solutions may be constructed by choosing different eigenvalues.

Since the analytic continuation of the low-Reynolds-number perturbation solution for $s = -1$ closely reproduces the numerical results of Lance and Rogers [4] and in the light of the foregoing discussion, there is little doubt that

the limit for large Reynolds number obtained by analytic continuation is the situation described by Stewartson. As Stewartson points out, Batchelor has not been proved wrong, but his limit is not realized either physically or by extending the solution for low Reynolds number. Perhaps, by analogy to the case where one disk is fixed, Batchelor's idea is a limit of another branch of solutions which begins at infinite Reynolds number. In view of Pearson's discovery at $R = 1000$, there appears to be no stable limit for this case of a continuation of the solution for low Reynolds number. Furthermore, the work of Tam [8] shows that through the existence of eigensolutions of the inviscid equations obtained as the limit for large Reynolds number, a core flow having multiple cells may exist for this case (at least mathematically) analogous to the situation found numerically by Mellor *et al.* for the case where only one disk rotates.

ACKNOWLEDGMENTS

The author is indebted to M. D. Van Dyke for his guidance and criticism and particularly for use of his unpublished results. The assistance of the McDonnell Douglas Corporation in preparing this manuscript is also gratefully acknowledged.

REFERENCES

1. G. K. BATCHELOR, *Quart. J. Mech. Appl. Math.* **4** (1951), 29.
2. T. VON KARMAN, *ZAMM* **1** (1921), 244.
3. K. STEWARTSON, *Proc. Cambridge Philos. Soc.* **49** (1953), 333.
4. G. N. LANCE AND M. H. ROGERS, *Proc. Roy. Soc. London, Ser. A* **266** (1962), 109.
5. E. H. BENTON, *Tellus* **20** (1968), 667.
6. C. E. PEARSON, *J. Fluid Mech.* **21** (1965), 623.
7. G. L. MELLOR, P. J. CHAPPLE, AND V. K. STOKES, *J. Fluid Mech.* **31** (1968), 96.
8. K. K. TAM, *SIAM J. Appl. Math.* **17** (1969), 1305.
9. G. H. HOFFMAN, Computer extension of some perturbation series in fluid mechanics, Ph.D. Thesis, Stanford University, Stanford, CA, 1970.
10. L. ROSENHEAD (Ed.), "Laminar Boundary Layers," Oxford University Press, London/New York, 1963.
11. C. DOMB AND M. F. SYKES, *Proc. Roy. Soc. London, Ser. A* **240** (1957), 214.
12. M. D. VAN DYKE, personal communication, 1970.
13. D. SHANKS, *J. Math. and Phys.* **34** (1955), 1.
14. G. A. BAKER, "Advances in Theoretical Physics" (K. A. Brueckner, Ed.), Vol. 1, p. 1, Academic Press, New York, 1965.
15. U. T. BÖDEWADT, *ZAMM* **20** (1940), 241.